

Spin transport through a spin-1/2 XXZ chain contacted to fermionic leads

Florian Lange,^{1,2} Satoshi Ejima,^{1,2} Tomonori Shirakawa,^{3,2,4,5} Seiji Yunoki,^{2,4,5} and Holger Fehske¹

¹*Institut für Physik, Ernst-Moritz-Arndt-Universität Greifswald, 17487 Greifswald, Germany*

²*Computational Condensed Matter Physics Laboratory,*

RIKEN Cluster for Pioneering Research (CPR), Saitama 351-0198, Japan

³*International School for Advanced Studies (SISSA), via Bonomea 265, 34136, Trieste, Italy*

⁴*Computational Quantum Matter Research Team,*

RIKEN Center for Emergent Matter Science (CEMS), Saitama 351-0198, Japan

⁵*Computational Materials Science Research Team,*

RIKEN Center for Computational Science (R-CCS), Hyogo 650-0047, Japan

(Dated: September 1, 2022)

We employ matrix-product state techniques to numerically study the zero-temperature spin transport in a finite spin-1/2 XXZ chain coupled to fermionic leads with a spin bias voltage. Current-voltage characteristics are calculated for parameters corresponding to the gapless XY phase and the gapped Néel phase. In both cases, the low-bias spin current is strongly suppressed unless the parameters of the model are fine-tuned. For the XY phase, this corresponds to a conducting fixed point where the conductance agrees with the Luttinger-liquid prediction. In the Néel phase, fine-tuning the parameters similarly leads to an unsuppressed spin current with a linear current-voltage characteristic at low bias voltages. However, with increasing the bias voltage, there occurs a sharp crossover to a region where a current-voltage characteristic is no longer linear and the smaller differential conductance is observed. We furthermore show that the parameters maximizing the spin current minimize the Friedel oscillations at the interface, in agreement with the previous analyses of the charge current for inhomogeneous Hubbard and spinless fermion chains.

I. INTRODUCTION

Besides the more usual semiconductor- and metal-based spintronics, there have been proposals to use magnetic insulators in spin-based devices¹⁻³. An advantage of these systems would be the absence of scattering due to conduction electrons, which may allow spin-current transmission over longer distances. Experiments have demonstrated the possibility to electrically induce a magnon spin current at a Pt/Y₃Fe₅O₁₂ interface by using the spin-Hall effect¹. More recently, a spin current has been driven through the spin-1/2-chain material Sr₂CuO₃ by applying a temperature gradient³. This was interpreted as a spinon spin current induced by the spin-Seebeck effect.

A lot of research has been reported on the spin transport in the antiferromagnetic spin-1/2 XXZ chain, especially concerning the question whether the dynamics are ballistic or diffusive in the linear-response regime. At zero temperature, it is known from the exact Bethe-ansatz calculations that the spin transport is ballistic in the gapless phase and diffusive in the gapped phase⁴. There is considerable analytical and numerical evidence that this also holds true at any finite temperature⁵⁻⁹. A possible exception is the $SU(2)$ isotropic point for which differing results have been obtained.

Here, we study the finite-bias spin transport for a specific setup with fermionic leads at zero temperature. To this end, we employ the density-matrix renormalization group (DMRG)¹⁰ and the real-time evolution of matrix-product states (MPS) via the time-evolving block decimation (TEBD)¹¹. The difference from previous studies of transport in finite spin chains is our choice of the leads.

In Refs. 12–14, boundary driving modeled by a Lindblad equation was considered, which allows the direct calculation of the non-equilibrium steady state with matrix-product-operator techniques. Interestingly, a negative differential conductance was observed for strong driving in the gapped phase. Other studies have explored the transport in inhomogeneous XXZ chains¹⁵ and fermionic quantum wires coupled to non-interacting leads, which map to an XXZ chain through a Jordan-Wigner transformation¹⁶⁻²⁰.

In setups with leads, the transport may be influenced by backscattering at the interfaces which, for repulsive interactions, can completely inhibit transport at low voltages and temperatures^{21,22}. In general, the strength of the backscattering will depend in a non-trivial way on the parameters on either side of the interface. In particular, it has been shown for typical models of fermionic chains that conducting fixed points with perfect conductance exist^{19,23,24}.

The primary concern of this paper is to numerically explore the possibility of such conducting fixed points for our specific setup of the junction. We consider both the gapless XY and the gapped Néel phase of the spin-1/2 XXZ chain. In the latter case, the energy gap leads to insulating behavior at zero temperature. One may then ask, how the insulating state breaks down at finite bias voltage and how the transport depends on the length of the chain. The charge transport in a similar setup with a Mott-insulating Hubbard chain has been addressed, e.g., in Ref. 25. Here, we show that conducting fixed points exist not only for gapless but, in as sense, also for gapped spin chains. However, beyond a low-bias region with nearly ideal conductance the current-voltage curves

at these fixed points are qualitatively different in the two regimes, with a smaller conductance in the gapped phase.

The rest of this paper is organized as follows. In Sec. II, we introduce the model and describe the numerical method employed. In Sec. III, we recapitulate some relevant field-theoretical results for the transport in inhomogeneous quantum wires. We then demonstrate in Sec. IV the existence of non-trivial conducting fixed points. To this end, we calculate steady-state spin currents and Friedel oscillations at the interface. In Sec. V, current-voltage curves for the gapless and the gapped regime are examined. Finally, Sec. VI summarizes our main results.

II. MODEL AND METHOD

We consider a spin-1/2 XXZ chain that is coupled via an exchange interaction to fermionic leads modeled by uniform tight-binding chains at half-filling. For simplicity, the exchange coupling between the spin chain and the leads is set to be identical to the exchange interaction inside the spin chain. The resulting Hamiltonian is

$$\hat{H}_0 = \hat{H}_S + \hat{H}_{L_1} + \hat{H}_{L_2} + \hat{H}_{S-L_1} + \hat{H}_{S-L_2}, \quad (1)$$

where

$$\hat{H}_S = J \sum_{j=1}^{N_s-1} \left[\frac{1}{2} \left(\hat{S}_j^+ \hat{S}_{j+1}^- + \hat{S}_j^- \hat{S}_{j+1}^+ \right) + \Delta \hat{S}_j^z \hat{S}_{j+1}^z \right] \quad (2)$$

describes the spin-1/2 XXZ chain containing N_s sites. As usual, \hat{S}_j^α is the α ($= x, y, z$) component of the spin-1/2 operator at site j , and $\hat{S}_j^\pm = \hat{S}_j^x \pm i\hat{S}_j^y$. The left (right) tight-binding lead is described by

$$\hat{H}_{L_1(L_2)} = -t \sum_{\sigma=\uparrow,\downarrow} \sum_{\substack{j<0 \\ (j>N_s)}} \left[\hat{c}_{j\sigma}^\dagger \hat{c}_{j+1,\sigma} + \hat{c}_{j+1,\sigma}^\dagger \hat{c}_{j\sigma} \right], \quad (3)$$

where $\hat{c}_{j\sigma}$ is the annihilation operator of an electron at site j with spin σ ($=\uparrow, \downarrow$). By defining the spin operators $\hat{S}_j^+ = \hat{c}_{j\uparrow}^\dagger \hat{c}_{j\downarrow}$, $\hat{S}_j^- = \hat{c}_{j\downarrow}^\dagger \hat{c}_{j\uparrow}$ and $\hat{S}_j^z = \frac{1}{2} (\hat{c}_{j\uparrow}^\dagger \hat{c}_{j\uparrow} - \hat{c}_{j\downarrow}^\dagger \hat{c}_{j\downarrow})$ at tight-binding sites j , the couplings between the spin chain and the left and right leads can be written as

$$\hat{H}_{S-L_1} = J \left[\frac{1}{2} \left(\hat{S}_0^+ \hat{S}_1^- + \hat{S}_0^- \hat{S}_1^+ \right) + \Delta \hat{S}_0^z \hat{S}_1^z \right], \quad (4)$$

and

$$\hat{H}_{S-L_2} = J \left[\frac{1}{2} \left(\hat{S}_{N_s}^+ \hat{S}_{N_s+1}^- + \hat{S}_{N_s}^- \hat{S}_{N_s+1}^+ \right) + \Delta \hat{S}_{N_s}^z \hat{S}_{N_s+1}^z \right], \quad (5)$$

respectively.

We now calculate the steady-state spin current that is generated by applying a spin bias voltage V . As in

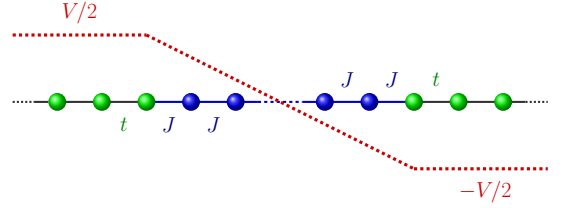


FIG. 1. Schematic depiction of the setup defined by the Hamiltonian $\hat{H}_0 + \hat{H}_V$ according to Eqs. (1) and (6). Blue (green) circles indicate the spin chain (left and right leads). The red dashed line denotes the spin bias potential, which linearly decreases inside the spin chain.

Ref. 25, the potential is assumed to drop off linearly in the spin chain, which adds the following term in the Hamiltonian (see also Fig.1):

$$\hat{H}_V = \sum_j V_j \hat{S}_j^z, \quad (6)$$

where

$$V_j = \begin{cases} \frac{V}{2}, & j \leq 0 \\ -\frac{V}{N_s+1}j + \frac{V}{2}, & 1 \leq j \leq N_s \\ -\frac{V}{2}, & j \geq N_s + 1. \end{cases} \quad (7)$$

The operator of the local spin-current is defined as

$$\hat{j}_j^z = \begin{cases} -\frac{it}{2} \hat{c}_j^\dagger \sigma_z \hat{c}_{j+1} + \text{h.c.}, & j < 0 \text{ or } j > N_s \\ \frac{iJ}{2} \hat{S}_j^+ \hat{S}_{j+1}^- + \text{h.c.}, & 0 \leq j \leq N_s, \end{cases} \quad (8)$$

where $\hat{c}_j^\dagger = (\hat{c}_{j\uparrow}^\dagger, \hat{c}_{j\downarrow}^\dagger)$ and σ_z is the z component of Pauli matrices²⁶. Our transport simulations are carried out in the zero-temperature limit. Then the system is initially in the ground state at time $\tau = 0$. More precisely, the time evolution is started from the ground state of \hat{H}_0 , where the spin chain and the leads are already coupled, and the spin bias voltage V is applied at $\tau = 0$. As discussed in Refs. 18 and 27, other setups are possible. For example, if one starts with the two leads decoupled from the spin chain and turns on the coupling, the transient behavior is different but the same steady-state properties are obtained. If, however, the system is in the ground state with a finite value of spin bias voltage V and the couplings \hat{H}_{S-L_1} and \hat{H}_{S-L_2} are switched on, different steady-state currents are expected for large V ²⁷.

For the numerical calculation of the steady-state current, we mostly follow the MPS-based approach of Refs. 18, 25, and 27. The DMRG and parallel TEBD are used, respectively, to calculate the ground state of \hat{H}_0 and simulate the time-evolution after the spin bias (described by \hat{H}_V) is switched on at $\tau = 0$. We employ a standard Suzuki-Trotter approximation where the Hamiltonian is decomposed into terms acting on even and odd bonds. Specifically, a second-order decomposition with time step $\delta\tau = 0.05/t$ is used. The leads have

to be truncated to finite length N_L , which gives rise to a discretization in the energy spectrum. The error due to this may be reduced by choosing appropriate boundary conditions with bond-dependent hopping strength that increase the energy resolution in the relevant energy region^{17,18}. Here, however, we find the leads with uniform hopping t to be sufficient.

In our calculation of the steady-state current, the accuracy is mainly limited by the accessible time scale. The finite size of the leads obviously restricts the simulations to the time until the current reflected at the open boundaries of the leads returns to the spin chain. Additionally, the entanglement growth of an out-of-equilibrium state requires an increase of the bond dimension m during the course of the time evolution, which eventually makes an accurate MPS representation of the state too costly. In the current setup, the von-Neumann entanglement entropy of the state after the perturbation grows linearly with the time²⁵, which requires an exponential increase of the bond dimension m for a fixed truncation error. The rate of the entanglement growth depends strongly on the applied voltage V . Simulation for large V are typically more expensive. We fix the truncation error to a maximum discarded weight 10^{-6} , which, in the worst cases, requires bond dimensions as large as $m = 2200$.

In principle, an MPS representation with one tensor for each site j in Eq. (1) could be used for all of our simulations. However, for small V , where larger lead sizes are necessary to get accurate results, we find it advantageous to split the tight-binding leads into two branches with different z component of the spin and employ a tree-tensor-network description²⁸ analogous to Ref. 29. This algorithm scales as m^4 at the interfaces, instead of m^3 , but the representation of the tight-binding leads becomes much more efficient, allowing us to simulate larger leads. In addition, the worse scaling of the bond dimension m is softened by the fact that the entanglement entropy at equilibrium is smallest at the interfaces, as already observed in Ref. 25.

III. LUTTINGER LIQUID DESCRIPTION

The low-energy physics of the spin-1/2 XXZ chain in the XY phase ($-1 \leq \Delta \leq 1$) are described by the Luttinger-liquid (LL) model³⁰

$$\hat{H}_s = \frac{1}{2} \int dx \left[\frac{v}{K} (\partial_x \phi)^2 + vK (\partial_x \theta)^2 \right], \quad (9)$$

where the bosonic fields obey the commutation relations $[\phi(x), \partial_{x'} \theta(x')] = i\delta(x - x')$ and the LL parameter $K = \pi/[2 \arccos(-\Delta)]$ and the spin velocity $v = J\pi\sqrt{1 - \Delta^2}/[2 \arccos(\Delta)]$ are known from the Bethe-ansatz solution³¹. The charge transport in a system of spinless fermions with a nearest-neighbor interaction corresponds directly to the spin transport in the spin-1/2 XXZ chain since the models are related by a Jordan-Wigner transformation. For an infinite homogeneous

chain, the spin conductance G is given by²²

$$G = \frac{K}{2\pi}. \quad (10)$$

In general, however, this expression is no longer valid when leads are taken into account. The effective low-energy Hamiltonian of the tight-binding leads in our setup described by Eq. (1) consists of two components of the form of Eq. (9) for the charge and spin sectors. Focusing only on the spin part, the naive field-theoretical description of our system becomes an inhomogeneous LL with the position-dependent LL parameter $K(x)$ and spin velocity $v(x)$. It has been shown that the conductance of such a system is obtained by replacing the LL parameter in Eq. (10) with its asymptotic value in the leads $K(x \rightarrow \pm\infty)$ ^{32,33}. For the non-interacting leads, the spin conductance therefore is $G = 1/(4\pi)$, independent of the parameters in the spin chain.

By using an inhomogeneous LL model to describe a one-dimensional junction one assumes that backscattering at the interfaces can be neglected. This is justified for adiabatic contacts but not for the abrupt transition between the spin chain and the lead described in Eq. (1). For a chain of spinless fermions with uniform LL parameter K , the effect of backscattering at an inhomogeneity on the conductance G is well-known^{21,22}: At zero temperature, G vanishes if the interactions are repulsive (i.e., $K < 1$), while G is not reduced for attractive interactions (i.e., $K > 1$). An abrupt change in the system parameters of a quantum wire has a similar impact on the conductance, as has been studied for both spinless^{19,23} and spinful²⁴ fermions using bosonization and quantum Monte Carlo methods. In those cases, whether the transport is suppressed at low temperatures depends on the LL parameters on each side of the interface. For the spinless model, the zero-temperature conductance vanishes for $\bar{K} < 1$, where $\bar{K} = 2(\frac{1}{K_1} + \frac{1}{K_2})^{-1}$, and K_1 and K_2 are the LL parameters on the left and right sides of the interface¹⁹. Assuming that this result holds for the spin part of our model in Eq. (1), the backscattering at the interface between the spin chain and the lead should be relevant for all values of anisotropy Δ , including negative values that correspond to $K > 1$. However, it was also shown that, even for abrupt junctions, conducting fixed points may be obtained by tuning certain system parameters such as the hopping and interaction strengths^{19,24}. At these conducting fixed points, the backscattering amplitude becomes zero and thus the ideal conductance determined by the LL parameters of the leads is recovered. We will show in the following section that similar conducting fixed points with ideal spin transport exist for the spin-chain junction described in Eq. (1). In fact, our model at the isotropic point with $\Delta = 1$ corresponds to a strong-coupling limit of the inhomogeneous Hubbard chain for which such a conducting fixed point has been reported in Ref. 24.

IV. CONDUCTING FIXED POINT

A. Spin current

To search for conducting fixed points, we simulate the spin transport at finite spin bias for the two-lead setup described in Eq. (1). Let us first illustrate the procedure used to obtain the steady-state spin current. Figure 2(a) shows the spin current profile for different time τ after the spin bias is switched on at $\tau = 0$. The current starts to flow in the spin chain and spreads over to the leads, where the wavefront moves with the Fermi velocity $2t$. While the spin current in the spin chain becomes position and time independent in a true steady state, we find it fluctuating even at the maximum simulated time. Therefore, here the steady-state value is estimated from the time dependence of the spin current $j_0^z(\tau)$ between the spin chain and the lead, as demonstrated in Fig. 2(b) for the isotropic chain. After a transient time of $\tau t \approx 10$, the spin current oscillates around its steady-state value with a period of approximately π/V . This kind of oscillation has been explained as a Josephson current that arises because of the finite size of the leads and the corresponding gap between the single-particle energy levels¹⁸. We calculate the steady-state value of the spin current either by simply averaging $j_0^z(\tau)$ over multiple periods of the oscillation or by adapting it to

$$j_0^z(\tau) = a_0 + a_1 \cos(2V\tau + a_2), \quad (11)$$

where a_0, a_1 and a_2 are fit parameters¹⁸.

The spin current generally depends on both the anisotropy Δ and the ratio J/t of the exchange interaction in the spin chain and the hopping amplitude in the leads. For most of the parameter space, the spin current is expected to be strongly suppressed because of the backscattering at the interfaces. As we will show, however, the system can be tuned to a conducting fixed point for each Δ by varying J/t . In the isotropic chain ($\Delta = 1$) considered in Fig. 2, for example, the corresponding value is $(J/t)_c \approx 2.4$. The current there is much larger than for the other values shown, $J/t = 1$ and $J/t = 3.4$, which lie away from the conducting fixed point.

The ratio J/t affects not only the steady-state value of the spin current but also the oscillation of the current as a function of time τ . For a fixed size of the leads with $N_L = 100$, the current oscillation at the interface is strongest at $J/t = (J/t)_c$ where it appears nearly undamped [see Fig. 2(b)]. For either larger or smaller value of J/t , on the other hand, the oscillation decays relatively quickly with increasing τ . By using the tree-tensor-network method, we also consider a junction with much larger leads of $N_L = 500$ sites. In this case, the current oscillation at the conducting fixed point becomes significantly smaller, as shown in Fig. 2(b), which confirms that it is mostly caused by the discretization of the single-particle energy levels in the leads¹⁸. The steady-state values of the spin current estimated from the simulations are the same for $N_L = 100$ and 500.

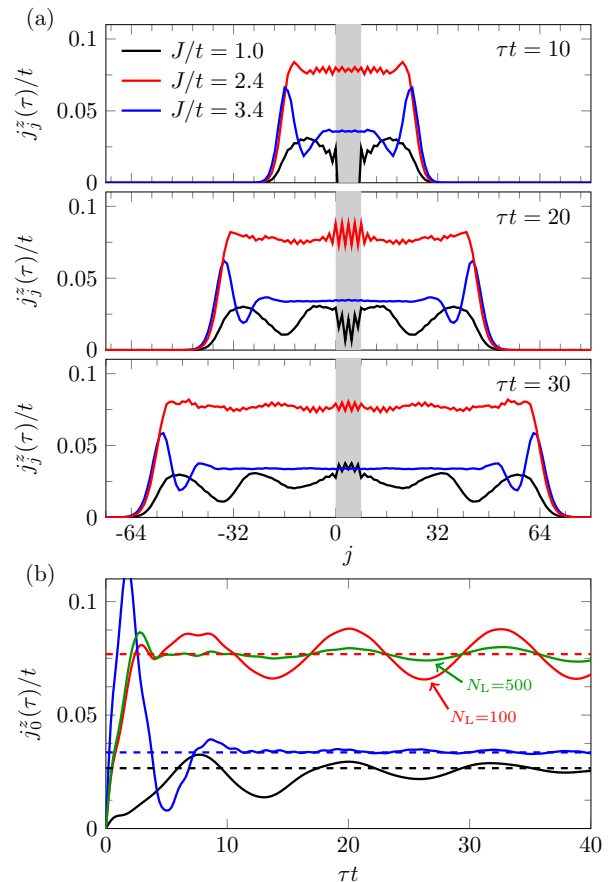


FIG. 2. Time evolution of the spin current $j_j^z(\tau)$ in a junction composed of an isotropic spin chain ($\Delta = 1$) of $N_s = 8$ sites (shaded region) coupled to tight-binding leads of $N_L = 100$ sites for spin bias $V/t = 1$ and several values of J/t . (a) Spin current profile at three different times $\tau t = 10, 20$, and 30. (b) Time dependence of the spin current $j_0^z(\tau)$ between the spin chain and the left lead (solid lines) and estimated steady-state value (dashed lines). The result for $J/t = 2.4$ with a larger size of the leads $N_L = 500$ is indicated by the green line.

Figure 3 shows the dependence of the steady-state spin current j^z on the ratio J/t at the fixed spin bias voltage $V/t = 0.2$ for several values of Δ . In each case, a clear maximum of the spin current appears. We first address the gapless phase for $\Delta = 1, 0$, and -0.5 where the LL description is applicable. For parameters in this regime, the maximum current obtained is close to that for a LL with adiabatic contacts, which indicates that a conducting fixed point with ideal linear conductance exists at the corresponding ratio $(J/t)_c$. As Δ is decreased, $(J/t)_c$ becomes larger. In addition, the current peak as a function of J/t broadens, which suggests that the backscattering becomes less relevant. A current maximum remains, however, even for negative Δ .

Figure 3 also shows the results for $\Delta = 2$ in the gapped phase. While a sharp peak is still observed, the maximum value of the spin current does not reach the ideal value in

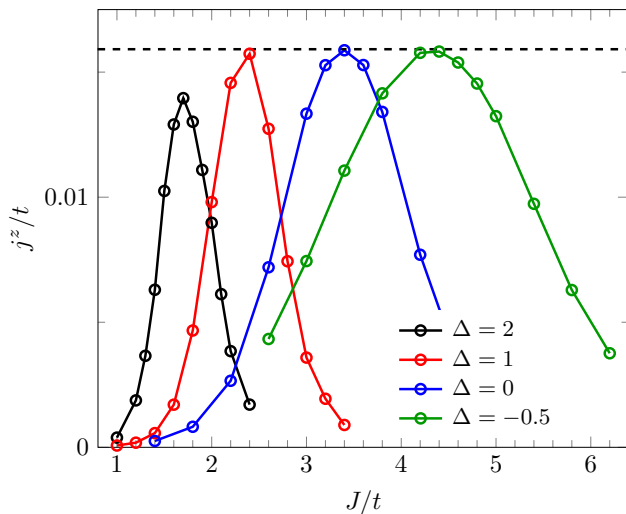


FIG. 3. Steady-state spin current j^z for four different values of Δ with varying J/t . Other parameters are $N_s = 8$, $N_L = 500$, and $V/t = 0.2$. The dashed line shows the current $V/(4\pi)$ expected for a Luttinger liquid with smooth interfaces.

this case. How the spin transport differs in the gapped and gapless phases of the antiferromagnetic XXZ chain will be analyzed in Sec. V.

B. Friedel oscillations

Besides its effect on the transport, the backscattering at inhomogeneities is known to induce characteristic Friedel oscillations of the local density or magnetization with twice the Fermi wavenumber k_F ³⁴. The Friedel oscillations at the interface vanish, however, if the backscattering amplitude is tuned to zero. The calculation of the magnetization profile therefore constitutes a different, perhaps more efficient way to search a conducting fixed point¹⁹. As a consistency check for the results of the spin-transport simulations above, we now investigate the dependence of the Friedel oscillations on J/t for fixed Δ with no spin bias applied. Since the magnetization is uniform in the spin-flip symmetric case, we examine the local susceptibility¹⁹ instead by adding a small uniform magnetic field described by $\delta\hat{H} = h\sum_j \hat{S}_j^z$. For these calculations, we consider a single interface between the tight-binding lead and the spin chain because the Friedel oscillations typically decay over a distance longer than the spin-chain length accessible in our transport simulations. Furthermore, we consider finite temperatures by using the grand-canonical purification method³⁵, which avoids problems in the convergence of the DMRG ground-state calculations. The purification method allows us to keep track of the growth of the Friedel oscillations starting from the interface and the open ends of the system as the temperature is lowered successively. We terminate the simulations when the finite system size begins to affect the results. The finite-temperature cal-

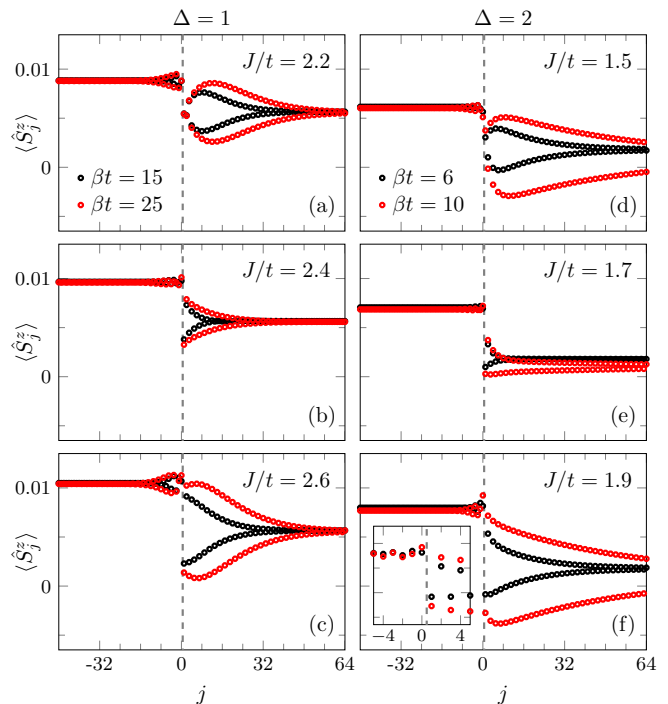


FIG. 4. Magnetization profile $\langle \hat{S}_j^z \rangle$ around the interface for an applied magnetic field $h/J = 0.05$. The dashed line indicates the interface between the tight-binding lead ($j \leq 0$) and the spin chain ($j > 0$). The system sizes are $N_L = 400$ and $N_s = 400$ for $\Delta = 1$ and $N_L = 400$ and $N_s = 800$ for $\Delta = 2$. The inset in (f) is a magnified view of the region close to the interface, highlighting the Friedel oscillations with wavenumber π . The results are obtained by finite temperature calculations at the inverse temperature β .

culations also allow us to study the gapped phase of the spin chain where the ground state is antiferromagnetically long-range ordered.

Figure 4 shows the magnetization profile around the interface for the magnetic field strength $h/J = 0.05$. Here, we fix h/J instead of h/t because for the values of the anisotropy Δ considered, the Friedel oscillations are much stronger in the spin chain than in the lead. Since the spin chain without magnetic field corresponds to a half-filled chain of fermions, the local magnetization oscillates with wavenumber $2k_F = \pi$. As expected, the effect is larger at low temperatures. For the fixed exchange anisotropy, the strength of the Friedel oscillations has a minimum as a function of J/t . This behavior can be observed in both the gapless and gapped regimes.

To measure the overall strength of the Friedel oscillations, we introduce a quantity

$$O_F = \sum_{j=1}^{N'} |\langle \hat{S}_{j+1}^z - \hat{S}_j^z \rangle|, \quad (12)$$

where N' is chosen so that the Friedel oscillations due to the open boundary at the end of the spin chain are excluded. By calculating O_F , we search for a value of

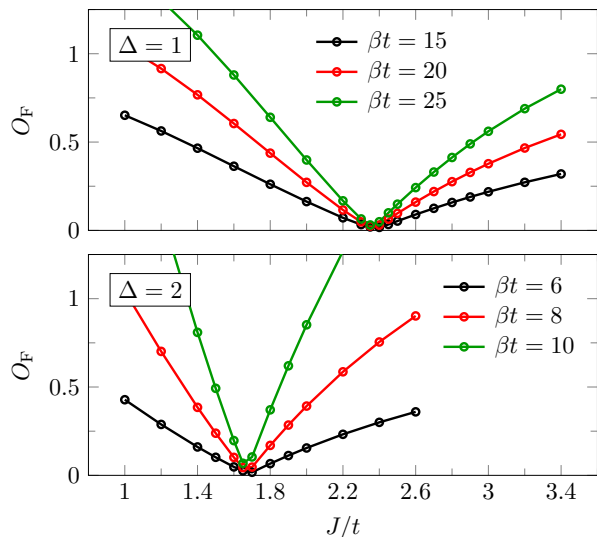


FIG. 5. Strength of the Friedel oscillations, O_F , defined in Eq. (12) around the interface inside the spin chain at the inverse temperature β . The system sizes are the same as in Fig. 4.

J/t that minimizes the Friedel oscillations for a fixed anisotropy Δ .

The results for $\Delta = 1$ and $\Delta = 2$ are shown in Fig. 5. In all cases studied, including the gapped regime, we find a clear minimum of the Friedel oscillation strength where approximately $O_F = 0$. When the temperature is lowered, the position of the minimum moves to smaller J/t . The temperature dependence seems to be stronger for small Δ . By identifying the position of the minimum for $T \rightarrow 0$ as the conducting fixed point, we obtain $(J/t)_c \approx 2.4$ for $\Delta = 1$. This value agrees with the results of the spin-transport simulations for $N_s = 8$, despite the fact that we now consider the limit of a large spin chain. Identifying $(J/t)_c$ similarly in the gapped phase, we obtain $(J/t)_c \approx 1.7$ for $\Delta = 2$, which also coincides with the value of J/t where the spin current becomes maximum in Fig. 3. When calculating $(J/t)_c$ as a function of the anisotropy Δ , we find no qualitative difference across the phase boundary at $\Delta = 1$.

V. CURRENT-VOLTAGE CHARACTERISTICS

Having established the existence of conducting fixed points with a finite linear conductance in the previous section, we now turn our attention to the spin bias dependence of the spin current. To examine how the current-voltage curve is modified by the backscattering at the interfaces and the presence of a finite energy gap, the system parameters at and away from the line of conducting fixed points are considered for both the gapless and gapped phases of the antiferromagnetic spin-1/2 XXZ chain.

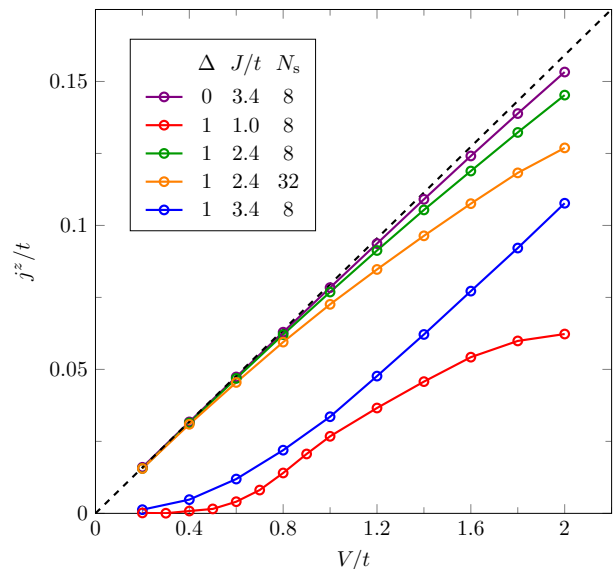


FIG. 6. Current-voltage curve in the two-lead setup described in Eq. (1) for different parameters in the gapless phase. The dashed line is the conductance $G = 1/(4\pi)$ of a Luttinger liquid smoothly connected to non-interacting leads.

A. Gapless regime

First, we study the gapless XY phase where the spin chain can be described by a LL model. As mentioned in Sec. III, a spin conductance $G = 1/(4\pi)$ is expected unless the transport is hindered by the backscattering at the interfaces. We have already confirmed that this ideal value can be obtained approximately at low spin bias $V/t = 0.2$ by tuning J/t to a conducting fixed point $(J/t)_c$ for a given anisotropy Δ . By calculating the current-voltage curve, we can determine at what energy scale the LL description becomes invalid and the linear behavior breaks down. Figure 6 shows the results for the isotropic spin chain ($\Delta = 1$) and the XX spin chain ($\Delta = 0$) where the conducting fixed points are $(J/t)_c \approx 2.4$ and $(J/t)_c \approx 3.4$, respectively (see Fig. 3 and Fig. 5). In both cases, the current-voltage curve for $J/t \approx (J/t)_c$ shows good agreement with the LL prediction up to at least $V/t = 1$, despite the strong inhomogeneity at the interfaces. For $\Delta = 1$, increasing the length of the spin chain to $N_s = 32$ leads to stronger deviations at large V while the currents for $V/t \lesssim 0.4$ remain nearly unchanged. Possible length-dependent corrections to the conductance have been considered, for example, in Refs. 36 and 37.

Away from the conducting fixed points, the low-bias conductance is strongly reduced by backscattering. This is demonstrated in Fig. 6 for an isotropic chain and values $J/t = 1$ and 3.4 that are significantly smaller or larger than $(J/t)_c \approx 2.4$. In a LL with an impurity, the differential conductance eventually approaches the ideal value $1/(4\pi)$ with a power law as the bias is increased³⁸. This is consistent with our results for $J/t = 3.4$ where an

approximately linear current-voltage relation is restored for $V/t \gtrsim 1.2$. For $J/t = 1$, on the other hand, the differential conductance drops off again at $V/t \approx 1$, likely because the bias voltage considered is already comparable or larger than the exchange constant J . In any case, the current should vanish in the large- V limit because of the finite bandwidth of the leads^{18,27}.

B. Gapped regime

In Sec. IV, it was shown that the finite temperature Friedel oscillations around the interfaces can be tuned to zero by varying J/t even in the gapped phase. Therefore, a fixed point $(J/t)_c$ with vanishing relevant backscattering seems to exist in this regime as well. One may then ask how the current-voltage curve there differs from that at a conducting fixed point in the gapless phase. In the following, we examine this for the anisotropy parameter $\Delta = 2$ where the Friedel oscillations disappear at $J/t \approx 1.7$.

Figure 7 displays the current-voltage curve of a spin chain with $N_s = 8$ sites for $J/t = 1.7$ as well as for smaller and larger values of J/t . For $J/t = 1.7$, the conductance appears to approach $1/(4\pi)$ as the voltage V is decreased to zero, suggesting that almost ideal spin transport can indeed be achieved at low energy. At larger voltage, on the other hand, the differential conductance drops off sharply, which is not observed in the LL phase. This crossover occurs approximately at $V/t \approx 0.4$. As in the LL regime, the spin current at small bias voltage is strongly reduced away from $(J/t)_c$. Since the XXZ spin chain with $\Delta > 1$ is a spin insulator in the thermodynamic limit, the spin transport should become increasingly suppressed with increasing the system size N_s . The effect of N_s on the current-voltage curve for $J/t = 1.7$ is shown in Fig. 8. As expected, the spin current becomes smaller when N_s is increased. There is still a crossover below which the perfect spin conductance seems to be approached. However, this crossover is shifted to smaller bias voltage V with N_s .

Similar behavior, i.e., unsuppressed current for small systems at low energy, occurs in the charge transport through Hubbard chains with an odd number of sites³⁹. Perhaps more relevant to our model, such effect has been predicted for one-dimensional charge-density-wave insulators adiabatically contacted to non-interacting leads, by using field theoretical methods²⁰. This model may be interpreted as a XXZ spin chain with the anisotropy Δ set to zero outside a finite region with $\Delta > 1$ that corresponds to the charge-density-wave part. In contrast to our results, a negative differential conductance was obtained. However, this may be related to the different choice of the leads.

For sufficiently long spin chains, we observe an upturn of the spin current at large spin bias. A setup analogous to ours has been considered in the calculation of the charge current through a Mott-insulating Hubbard chain

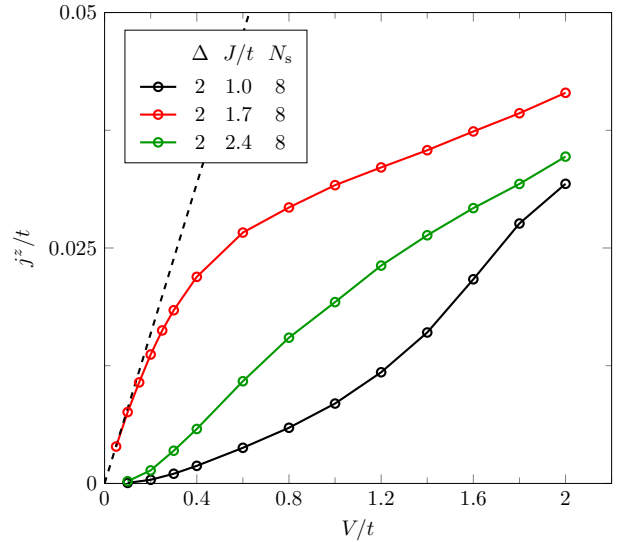


FIG. 7. Current-voltage curve for a spin chain with $N_s = 8$, anisotropy $\Delta = 2$, and different values of J/t . The dashed line corresponds to the ideal conductance $G = 1/(4\pi)$ obtained in the Luttinger-liquid regime.

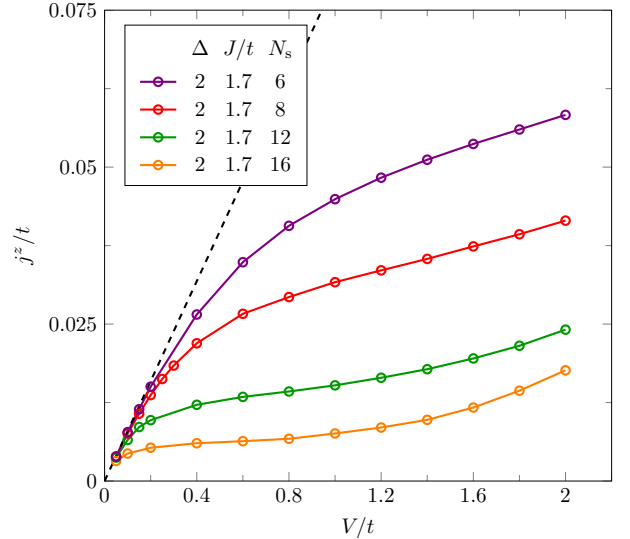


FIG. 8. Same as in Fig. 7 but for a spin chain with $J/t = 1.7$ and various chain lengths.

connected to non-interacting leads²⁵. It was shown that the current-voltage curve can be described by a function $j(V) = aV e^{-V_c/V}$, where a and V_c are constants. In particular, V_c is approximately proportional to the square of the charge gap of the disconnected Hubbard chain. This relation was previously obtained for the current in a periodic chain and explained in terms of a Landau-Zener mechanism⁴⁰. The upturn observed for $N_s = 16$ in Fig. 8 suggests that a similar activated behavior occurs in our model for long enough chains where the low-voltage transport is suppressed. However, our available data is not sufficient to check the specific functional form and the

dependence on the spin gap of the isolated spin chain.

VI. CONCLUSION

We have numerically studied the finite-bias spin transport in a spin-1/2 XXZ chain connected to half-filled tight-binding leads at zero temperature, focusing on the effect of scattering at the interfaces. By calculating the steady-state spin current and the Friedel oscillations, it was shown that in the LL regime, conducting fixed points with the ideal linear conductance exist, similarly as in related models for inhomogeneous quantum wires. Our results furthermore indicate that conducting fixed points also appear in the gapped phase. There, however, the nearly ideal spin transport can only be observed in a small bias voltage region, which shrinks when the length of the spin chain is increased.

More difficult to treat numerically, but closer to actual experiments, is the finite temperature case. For the finite-temperature simulations, one could employ a similar TEBD method where the MPS describes a purification of the density matrix instead of a pure state. With the approach in Ref. 41, it may also be possible to study a setup where a spin current is driven by a temperature

gradient, mimicking the experiment in Ref. 3.

Here, we have only considered junctions composed of spin-1/2 chains. A possible extension would be to study analogous systems for spin ladders or chains with higher local spin. The spin-1 Heisenberg chain, for example, might be interesting since it is experimentally realizable and differs from the spin-1/2 chain in several aspects: Its elementary excitations are magnons instead of spinons, it is non-integrable, and it exhibits symmetry-protected edge states at open boundaries. For a setup with leads, the question then arises how the contact is affected by these edge states.

ACKNOWLEDGMENTS

DMRG simulations were performed using the ITensor library⁴². F. L. was supported by Deutsche Forschungsgemeinschaft through project FE 398/8-1 and by the International Program Associate (IPA) program in RIKEN. This work was supported by Grant-in-Aid for Scientific Research from MEXT Japan under the Grant No. 17K05523 and also in part by HPCI Strategic Programs for Innovative Research (SPIRE) (Nos. hp120246, hp140130, and hp150140). T. S. acknowledges the Simons Foundation for funding.

-
- ¹ Y. Kajiwara, K. Harii, S. Takahashi, J. Ohe, K. Uchida, M. Mizuguchi, H. Umezawa, H. Kawai, K. Ando, K. Takanashi, S. Maekawa, and E. Saitoh, *Nature* **464**, 262 (2010).
- ² K. Uchida, H. Adachi, T. Ota, H. Nakayama, S. Maekawa, and E. Saitoh, *Appl. Phys. Lett.* **97**, 172505 (2010).
- ³ D. Hirobe, M. Sato, T. Kawamata, Y. Shiomi, K. Uchida, R. Iguchi, Y. Koike, S. Maekawa, and E. Saitoh, *Nat. Phys.* **13**, 30 (2016).
- ⁴ B. S. Shastry and B. Sutherland, *Phys. Rev. Lett.* **65**, 243 (1990).
- ⁵ X. Zotos, *Phys. Rev. Lett.* **82**, 1764 (1999).
- ⁶ F. Heidrich-Meisner, A. Honecker, D. C. Cabra, and W. Brenig, *Phys. Rev. B* **68**, 134436 (2003).
- ⁷ M. Žnidarič, *Phys. Rev. Lett.* **106**, 220601 (2011).
- ⁸ C. Karrasch, J. Hauschild, S. Langer, and F. Heidrich-Meisner, *Phys. Rev. B* **87**, 245128 (2013).
- ⁹ T. Prosen, *Phys. Rev. Lett.* **106**, 217206 (2011).
- ¹⁰ S. R. White, *Phys. Rev. Lett.* **69**, 2863 (1992).
- ¹¹ G. Vidal, *Phys. Rev. Lett.* **91**, 147902 (2003).
- ¹² T. Prosen and M. Žnidarič, *J. Stat. Mech.: Theor. Exp.* **2009**, P02035 (2009).
- ¹³ G. Benenti, G. Casati, T. Prosen, D. Rossini, and M. Žnidarič, *Phys. Rev. B* **80**, 035110 (2009).
- ¹⁴ G. Benenti, G. Casati, T. Prosen, and D. Rossini, *Europhys. Lett.* **85**, 37001 (2009).
- ¹⁵ K. A. van Hoogdalem and D. Loss, *Phys. Rev. B* **84**, 024402 (2011).
- ¹⁶ P. Schmitteckert, *Phys. Rev. B* **70**, 121302 (2004).
- ¹⁷ D. Bohr, P. Schmitteckert, and P. Wölfle, *Europhys. Lett.* **73**, 246 (2006).
- ¹⁸ A. Branschädel, G. Schneider, and P. Schmitteckert, *Ann. Phys. (Berlin)* **522**, 657 (2010).
- ¹⁹ N. Sedlmayr, J. Ohst, I. Affleck, J. Sirker, and S. Eggert, *Phys. Rev. B* **86**, 121302 (2012).
- ²⁰ V. V. Ponomarenko and N. Nagaosa, *Phys. Rev. Lett.* **83**, 1822 (1999).
- ²¹ C. L. Kane and M. P. A. Fisher, *Phys. Rev. Lett.* **68**, 1220 (1992).
- ²² C. L. Kane and M. P. A. Fisher, *Phys. Rev. B* **46**, 15233 (1992).
- ²³ N. Sedlmayr, D. Morath, J. Sirker, S. Eggert, and I. Affleck, *Phys. Rev. B* **89**, 045133 (2014).
- ²⁴ D. Morath, N. Sedlmayr, J. Sirker, and S. Eggert, *Phys. Rev. B* **94**, 115162 (2016).
- ²⁵ F. Heidrich-Meisner, I. González, K. A. Al-Hassanieh, A. E. Feiguin, M. J. Rozenberg, and E. Dagotto, *Phys. Rev. B* **82**, 205110 (2010).
- ²⁶ R. A. Bari, D. Adler, and R. V. Lange, *Phys. Rev. B* **2**, 2898 (1970).
- ²⁷ M. Einhellinger, A. Cojuhovski, and E. Jeckelmann, *Phys. Rev. B* **85**, 235141 (2012).
- ²⁸ V. Murg, F. Verstraete, O. Legeza, and R. M. Noack, *Phys. Rev. B* **82**, 205105 (2010).
- ²⁹ A. Holzner, A. Weichselbaum, and J. von Delft, *Phys. Rev. B* **81**, 125126 (2010).
- ³⁰ T. Giamarchi, *Quantum physics in one dimension* (Clarendon Press, Oxford, 2003).
- ³¹ A. Luther and I. Peschel, *Phys. Rev. B* **12**, 3908 (1975).
- ³² D. L. Maslov and M. Stone, *Phys. Rev. B* **52**, R5539 (1995).
- ³³ I. Safi and H. J. Schulz, *Phys. Rev. B* **52**, R17040 (1995).

- ³⁴ S. Rommer and S. Eggert, Phys. Rev. B **62**, 4370 (2000).
- ³⁵ F. Verstraete, J. J. García-Ripoll, and J. I. Cirac, Phys. Rev. Lett. **93**, 207204 (2004).
- ³⁶ N. Sedlmayr, P. Adam, and J. Sirker, Phys. Rev. B **87**, 035439 (2013).
- ³⁷ K. A. Matveev and A. V. Andreev, Phys. Rev. Lett. **107**, 056402 (2011).
- ³⁸ M. P. A. Fisher and L. I. Glazman, “Transport in a One-Dimensional Luttinger Liquid,” in *Mesoscopic Electron Transport*, edited by L. L. Sohn, L. P. Kouwenhoven, and G. Schön (Springer Netherlands, Dordrecht, 1997) pp. 331–373.
- ³⁹ A. Oguri, Phys. Rev. B **63**, 115305 (2001).
- ⁴⁰ T. Oka, R. Arita, and H. Aoki, Phys. Rev. Lett. **91**, 066406 (2003).
- ⁴¹ C. Karrasch, R. Ilan, and J. E. Moore, Phys. Rev. B **88**, 195129 (2013).
- ⁴² <http://itensor.org/>.